Electrochemical Behavior and Redox-Dependent Disassembly of Gallic Acid/Fe^{III} Metal–Phenolic Networks

Pavel V. Cherepanov,[†] Md. Arifur Rahim,[†] Nadja Bertleff-Zieschang,[†] Md. Abu Sayeed,[‡] Anthony P. O'Mullane,[‡] Simon E. Moulton,[§] and Frank Caruso[†]*

[†]ARC Centre of Excellence in Convergent Bio-Nano Science and Technology, and the Department of Chemical Engineering, The University of Melbourne, Parkville, Victoria 3010, Australia

[‡]School of Chemistry, Physics and Mechanical Engineering, Queensland University of Technology (QUT), Brisbane, Queensland 4001, Australia

[§]ARC Centre of Excellence for Electromaterials Science, Faculty of Science, Engineering and Technology, Swinburne University of Technology, Hawthorn, Victoria 3122, Australia

*Corresponding author. E-mail: fcaruso@unimelb.edu.au

ABSTRACT

Metal–phenolic networks (MPNs) are a versatile class of organic–inorganic hybrid systems that are generating interest for application in catalysis, bio-imaging, and drug delivery. These self-assembled MPNs possess metal-coordinated structures and may potentially serve as redox-responsive platforms for triggered disassembly or drug release. Therefore, a comprehensive study of the reduction and oxidation behavior of MPNs for evaluating their redox-responsiveness, specific conditions required for the disassembly, and the kinetics of metal ion release is necessary. Using a representative MPN gallic acid–iron (GA/Fe^{III}) system, we conducted electrochemical studies to provide valuable fundamental insights into the redox behavior of these MPN networks. We demonstrate that GA/Fe^{III} is redox active, and evaluate its electrochemical reversibility, identify the oxidation state of the redox active species, and provide information regarding the stability of the networks toward reductive stimuli and specific redox conditions required for the "on–off" or continuous release of Fe^{III}. Overall, through studying the redox properties of GA/Fe^{III} films, we advance the understanding of multifunctional iron-containing MPN platforms that may have practical significance for biologically relevant applications.

INTRODUCTION

Functional hierarchical materials fabricated using coordination-driven self-assembly are of importance in diverse fields of materials science.[1–4] Among these is the recently reported versatile class of organic–inorganic hybrid systems known as metal–phenolic networks (MPNs).[5] Typically, MPNs are formed using naturally abundant phenolic compounds bearing catechol or galloyl groups and transition metals as structural motifs.[5–10] The formation of MPNs on a solid substrate involves the interfacial assembly of strongly coordinated metal–phenolic complexes resulting in stable, surface-confined amorphous films. Advancing from the initial

use of tannic acid as a macromolecular polyphenolic ligand,[5,7] the MPN assembly process has been observed to be more generic in nature and applicable to simpler phenolic moieties such as gallic acid (GA), pyrogallol, and pyrocatechol.[9] MPN films formed from these simple phenolic ligands and Fe^{III} have provided valuable insights into the structural requirements for the assembly process and details on the coordination chemistry of the resulting networks.[9] Moreover, these findings have guided the design of iron-containing MPNs from other small biologically functional ligands such as quercetin and myricetin.[11]

To date, MPNs have shown potential applications in various fields such as catalysis, separations, bio-imaging, and drug delivery.[7,12–14] Although progress has been made in understanding the assembly, structure, and physicochemical properties of MPN films,[5,7,9,15] the electrochemical nature of MPNs, such as reduction and oxidation behavior, has received scant attention.[16] In general, *ortho*-dihydroxybenzenes (i.e., catechol) are known to be redox active in both their pristine (i.e., non-coordinated form) and coordinated forms in discrete metal complexes.[17–19] Thus, it can be expected that the coordinated structures of MPNs will respond to electrochemical stimuli and that such responses will add to our current understanding of the nature of the coordination networks. In particular, the electrochemical analysis of MPN systems may provide details on specific characteristics such as redox activity and reversibility, the oxidation states of the redox-active species, and specific conditions required for controlled disassembly. Overall, understanding the reduction and oxidation properties of MPNs may provide valuable fundamental insights for the future design of electrochemical actuators, which are important for applications such as controlled drug release.[20–25] Additionally, precise redox-dependent control of the disassembly of iron-containing MPNs may be useful in environments such as soils, and fresh and marine waters where the bioavailability of iron is compromised because of its poor solubility.[26,27] Therefore, MPNs also have the potential to serve as an iron-controlling platform for agri/aquaculture and marine science.[28,29]

Herein, we focused on the electrochemical behavior of an MPN system prepared using a simple and naturally abundant phenolic ligand, GA, and Fe^{III} as the metal crosslinker. Electrochemical characterization was performed using cyclic voltammetry and chronoamperometry techniques under both static and dynamic conditions. The as-prepared GA/Fe^{III} MPN system was found to be redox responsive, and its electrochemical response could be correlated to the specific coordination interactions between the structural motifs. We also analyzed the reversibility of the electrochemical response and provide details on the nature of the redox-active species within the GA/Fe^{III} networks. Additionally, we report on the possible release of Fe^{III} from the networks triggered by electrochemical stimuli and demonstrate the specific redox conditions required for the continuous disassembly of the GA/Fe^{III} networks.

EXPERIMENTAL SECTION

Materials. Gallic acid (GA, 97.5%), iron(III) chloride hexahydrate (FeCl$_3$·6H$_2$O), sodium hydroxide (NaOH), and sodium sulfate (Na$_2$SO$_4$) were purchased from Sigma-Aldrich and used as received. Polystyrene (PS) particles (diameter = 3.20 ± 0.07 μm) were purchased from microParticles GmbH. Tetrahydrofuran (THF) was purchased from Chem-Supply. High-purity (Milli-Q) water with a resistivity of 18.2 MΩ cm was obtained from an inline Millipore RiOs/Origin water purification system.

GA/Fe^{III} Film Formation on Particulate Substrates. The standard protocol is described as follows. First, 50 μL of the PS particles (10% (w/w) water suspension) was washed twice with Milli-Q water. Then, 400 μL of the ligand (GA) solution (15 mM) was added to the PS particle suspension and vortexed for 10 s. Subsequently, 200 μL of FeCl$_3$·6H$_2$O (30 mM) solution was added and quickly vortexed for 3−4 s. The pH of the mixture was raised by adding 20 μL of NaOH solution (0.5 M), followed by vortexing for 1 min; the final pH of the mixture

was ~3.8. Unreacted supernatant was removed by centrifugation (1700 g, 1 min) followed by four washing steps in Milli-Q water. Dissolution of the PS cores was accomplished by washing the pellets with THF thrice (1900 g, 1 min). The obtained hollow capsules were washed twice (2000 g, 3 min) with Milli-Q water and finally resuspended in 400 µL of Milli-Q water for characterization.

Sample Preparation for the Electrochemical Measurements. The total amount of freshly prepared GA/Fe^{III} capsules yielded (~2 × 10^6, determined from the final capsule dispersion by flow cytometry) was resuspended in 2.5 µL/25 µL nafion/ethanol solution. Then, 10 µL of the resulting GA/Fe^{III} capsule suspension was drop-cast onto either a glassy carbon electrode (GCE) or a rotating ring-disk electrode (RRDE) and air-dried. Before each drop-casting procedure, both the GCE and RRDE were thoroughly polished using an alumina polishing kit and washed with ethanol. Cyclic voltammograms on the GCE were recorded in the potential region ranging from −500 to +900 mV for the GA/Fe^{III} systems and from −900 to +900 mV for the 15 mM gallic acid solution. In each case, the scan rate was 5 mV/s. Cyclic voltammograms of the GA/Fe^{III} system on the RRDE were recorded in the potential regions ranging from −450 to +700 mV and from +150 to +700 mV. In each case, the scan rate was 10 mV/s. Chronoamperograms were recorded at the gold ring electrode at a constant potential of −450 mV.

Characterization. Differential interference contrast microscopy images were taken with an inverted Olympus IX71 microscope. The number of capsules was counted using an Apogee A50-Micro flow cytometer (Apogee Flow Systems, UK). Electrochemical experiments under static conditions were performed using a MM510 potentiostat/galvanostat (MMates, Italy). For the cyclic voltammetry measurements, a standard three-electrode electrochemical cell that comprised a GCE (diameter = 3 mm), a Pt wire, and Ag/AgCl(KCl) as the working, counter, and reference electrodes, respectively, was used. For all

electrochemical measurements, 1 M Na_2SO_4 aqueous solution was used as the supporting electrolyte. The supporting electrolyte was deaerated by purging nitrogen for 30 min before each measurement. Electrochemical experiments under dynamic conditions were performed using an Autolab bipotentiostat/galvanostat (BioLogic VSP workstation). A similar three-electrode electrochemical cell setup was used to record the cyclic voltammograms and chronoamperograms with the exception of using a rotating ring-disk (BAS) as the working electrode (RRDE, glassy carbon disk – 4 mm diameter, gold ring width – 2 mm, gap between outer circle of the disk and inner circle of the ring – 1 mm). The rotating speed was set to 1000 rpm.

RESULTS AND DISCUSSION

GA/Fe^{III} capsules were prepared using a coordination-driven self-assembly approach according to our previous report.[9] Briefly, polystyrene (PS) templates (diameter ~3.2 μm) were mixed with an aqueous solution of GA followed by the addition of an aqueous Fe^{III} salt solution in a stoichiometric ratio of 1:1. After washing the GA/Fe^{III}-coated PS templates, the templates were dissolved using THF to obtain the GA/Fe^{III} capsules (**Figure S1**, Supporting Information). Full characterization of this system can be found elsewhere.[9] To study the electrochemical behavior, freshly prepared GA/Fe^{III} capsules were resuspended in an ethanol/nafion solution, drop-cast on a GCE, and air-dried. Colloidal MPN films (i.e., capsules) were fabricated with a high degree of precision and homogenous film thickness.[9] We used the capsules throughout this study to ensure the consistency of the deposited amount on the GCE. Note that, the electrochemical behavior of planar and colloidal films has been reported to be identical.[30–32]

Figure 1a, b schematically shows the synthesis of the GA/Fe^{III} capsules and their preparation for the electrochemical studies. The cyclic voltammogram (CV) of the GA/Fe^{III} system, which was recorded in the potential region ranging from −500 to +900 mV, is shown

in **Figure 1**c. This potential window was chosen to reduce or potentially exclude any possible competitive processes of hydrogen and oxygen evolution[33,34] that might affect the electrochemical data evaluation. It is well established that such competitive processes for many of the materials studied in the literature occur outside of this selected range.[33,35] As observed from the recorded CV (**Figure 1**c), the GA/Fe^{III} networks exhibited a well-pronounced redox response, with distinct oxidation and reduction processes when compared to the CV recorded at a bare GCE (**Figure 1**c, black dotted line). In the forward scan from 0 to +900 mV, the oxidation of GA/Fe^{III} began at a low potential of +80 mV and proceeded until a current density value of ~0.11 mA/cm^2 was attained. During the reverse scan from +900 to −500 mV, a reduction peak at +80 mV with a much lower current density of approximately −0.02 mA/cm^2 appeared. The observed difference (about 5-fold) in the absolute values recorded for the oxidation and reduction processes (i.e., 0.11 vs −0.02 mA/cm^2) might be related to the origin of the redox-active species. Thus, the redox behavior of the GA/Fe^{III} networks observed in the initial CV cycle, at the given scan rate (5 mV/s) and the chosen potential window, can be attributed to either (i) the presence of a specific redox-responsive structural motif in the GA/Fe^{III} networks, though its reduction and oxidation kinetics vary, or (ii) the presence of several structural motifs, which are responsible for the redox activity. More details regarding the redox-responsive structural aspects of the GA/Fe^{III} networks are provided below.
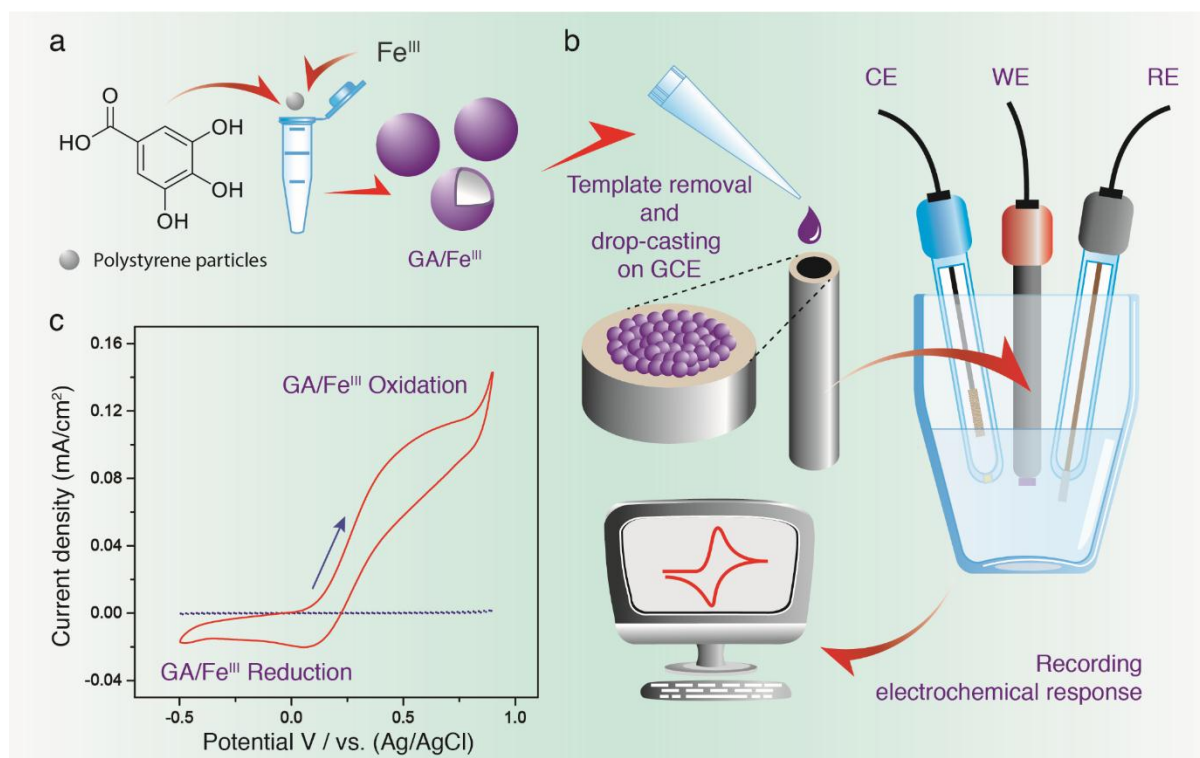
Figure 1. (a) Schematic representation of the synthesis of the GA/Fe^{III} networks and (b) an overview of the experimental setup used for its electrochemical characterization. (c) Cyclic voltammogram of the GA/Fe^{III} networks recorded under static conditions in an aqueous solution of 1 M Na$_2$SO$_4$. The cyclic voltammogram (dotted line) of a bare glassy carbon electrode used as the reference is also shown. The arrow indicates the direction of the CV scan. The scan rate was 5 mV/s. GCE, glass carbon electrode; CE, counter electrode; WE, working electrode; RE, reference electrode.

To determine the origin of redox-responsiveness of the GA/Fe^{III} networks, the CV of the pristine GA solution (**Figure 2**a) was recorded and used as a reference. Two distinct oxidation peaks at +350 and +650 mV were observed. The first peak observed at the lower potential was attributed to the oxidation of the catechol group (denoted by the triangle in **Figure 2**a) present in GA to a quinone motif, whereas the second peak (observed at the higher potential) originated from the oxidation of the residual (other than catechol) single hydroxyl groups (denoted by the asterisks in **Figure 2**a). These observations agree well with previously

reported electrochemical data for GA and similar phenolic compounds.[17,36] Based on the position of the oxidation peak and the corresponding higher current density value associated with the oxidation of the catechol groups (when compared with that observed for the oxidation of other −OH groups), it is suggested that the oxidation of the catechol group of GA to quinone is the dominant process. Moreover, the oxidation of GA as a whole is an irreversible process, and no related reduction peaks were observed (**Figure 2**a). This observation indicates that the oxidation response (as mentioned earlier) of the GA/Fe^{III} networks, upon the first forward scan, primarily originates from the phenolic ligand. This observation is additionally supported by the fact that GA/Fe^{III} capsules contain iron in the oxidation state of +3;[9,37] in this oxidation state, iron is highly unlikely to be oxidized further.
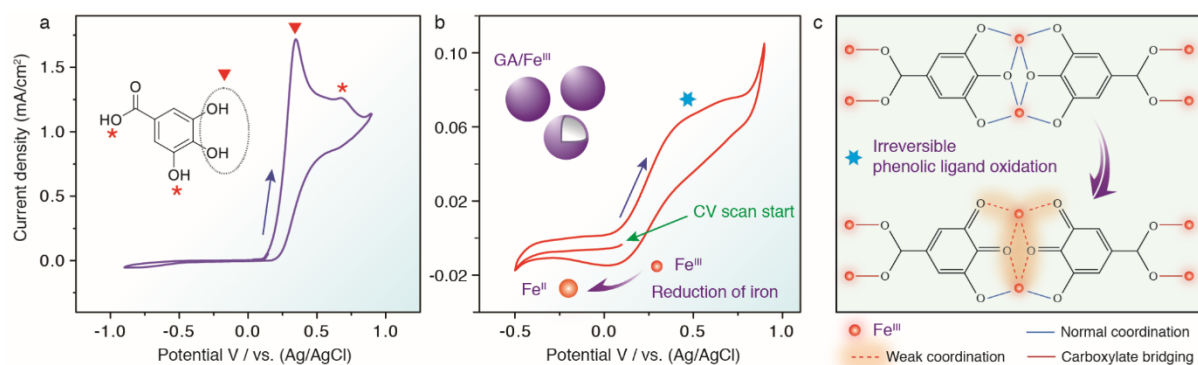

Figure 2. Cyclic voltammograms of (a) a 15 mM GA aqueous solution at a bare GCE and (b) the GA/Fe^{III} networks recorded under static conditions. Triangles and asterisks in (a) denote oxidation of catechol and residual hydroxyl groups respectively. The CV in (b) was originally swept from +100 to −500 mV followed by a complete cycle. The blue arrows in (a) and (b) indicate the direction of the scan. The green arrow in (b) shows the start of the scan. The scan rate was 5 mV/s. (c) Schematic representation of the possible oxidation of GA in the GA/Fe^{III} networks, assuming that the irreversible oxidation of the catechol group of GA to quinone dominates the process.

9

Because the phenolic ligand is irreversibly oxidized, we suggest that the peak observed in the reverse scan of the GA/Fe^{III} networks (**Figure 1**c) originates from the reduction of Fe^{III} to Fe^{II}. To investigate this further, the CV of GA/Fe^{III} was recorded at a scanning potential range between +100 and −500 mV first, followed by an additional complete CV cycle (**Figure 2**b). The starting potential of +100 mV was selected to avoid oxidation of GA within the GA/Fe^{III} networks. As expected, because of the possible shift in redox potential of the coordinated metal ions,[38,39] no reduction peaks were observed despite the presence of Fe^{III} within the networks, which could potentially be reduced to Fe^{II}. Furthermore, it is known that Fe^{III} ions are strongly coordinated to the phenolic ligands in the GA/Fe^{III} networks (**Figure 2**c), and therefore, they are possibly not responsive to the reductive stimuli in the chosen potential scan range studied. Interestingly, the reduction peak only appeared upon completion of the consecutive oxidation scans. This finding can be explained by the irreversible oxidation of the catechol groups to quinones at the more positive potential, as determined from analysis of the pristine GA solution. Even after oxidation, Fe^{III} remains coordinated to the quinone groups, which possibly maintains the structural integrity of the networks (**Figure 2**c), however, to a significantly weaker degree when compared to the pristine GA/Fe^{III} complexes[40] in the networks. Accordingly, the metal ions are available for reduction. Overall, based on the obtained electrochemical data, the redox response of the GA/Fe^{III} networks originates from different structural motifs, with the GA ligand being oxidized and, therefore, fostering weaker Fe^{III}–ligand interactions and allowing the Fe^{III} ions to be reduced during the first complete CV scan.

To further evaluate the redox behavior of the GA/Fe^{III} system, especially upon irreversible oxidation of the phenolic ligands, five consecutive CV cycles were run in the potential range starting from −500 to +900 mV. As observed in **Figure 3**a, the redox response of the GA/Fe^{III} networks is of a quasi-reversible character, that is, oxidation and reduction

peaks were clearly identifiable in all cycles, although, with a noticeable decrease in the current magnitude when compared to the 1st CV cycle. Substantial decreases in the current, especially for the oxidation peak, were observed between the 1st and 2nd cycles as well as between the 2nd and 3rd cycles. After the 3rd cycle, changes in the current were minimal. Hence, the current density values for the 4th and 5th CV cycles were comparable. The decrease in the oxidation peak current between the 1st and 2nd CV cycles was attributed to the irreversible oxidation of GA in the GA/Fe^{III} networks. The oxidation peak observed in the 2nd CV cycle most likely originated from both the (i) remaining non-oxidized catechol groups of the GA/Fe^{III} networks and (ii) oxidation of Fe^{II} to Fe^{III} after its reduction in the 1st CV cycle. The same scenario is expected to occur for all subsequent CV cycles until the oxidation of GA is complete and only the quasi-reversible (the peak-to-peak separation is greater than 59 mV)[39] oxidation/reduction of Fe^{II}/Fe^{III}–quinone complex is observed (**Figure 3**b). Assuming that the last statement is valid for the 5th CV cycle, we attempted to estimate the oxidized portion of GA upon completion of each CV cycle. **Figure 3**b shows changes in the residual oxidation current as a function of the cycle number. The current exponentially decayed to about 20% of its original value. This decrease can be attributed to the quasi-reversible Fe^{II}-to-Fe^{III} oxidation response in all CV cycles except for the 1st cycle, as noted earlier. Therefore, for a given amount of GA/Fe^{III} sample, ~80% of GA is irreversibly oxidized after completion of the 1st CV cycle (region (I) in **Figure 3**b), while the remaining 20% of GA is oxidized over the next three CV cycles (region (II) in **Figure 3**b). Region (III) in **Figure 3**b represents Fe^{II}-to-Fe^{III} oxidation. Also, the reduction peak current decreased after completion of the 1st CV cycle. Although the decrease in magnitude was not as drastic as that observed for the oxidation peak (**Figure S2**), we assumed that the decrease occurred possibly because of partial release of the metal ions from the GA/Fe^{III} networks during the applied electrochemical stimuli.
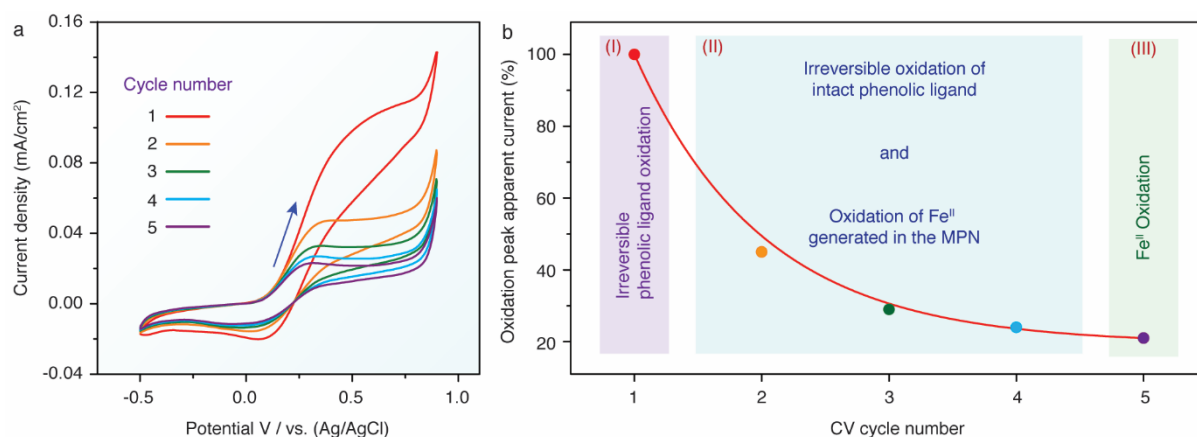
Figure 3. (a) Successive cyclic voltammograms of the GA/Fe^{III} networks recorded under static conditions. The arrow indicates the direction of the scan. (b) Changes in the residual oxidation peak current as a function of the cycle number. The scan rate was 5 mV/s.

To support the hypothesis that iron ions are released from the GA/Fe^{III} networks during oxidation, the experimental setup was altered accordingly for additional electrochemical characterization studies. Specifically, the conventional GCE used under static conditions was replaced with a RRDE onto which the suspension of GA/Fe^{III} capsules in ethanol/nafion solution was drop-cast onto the disc portion of the electrode and air-dried (**Figure 4**a). The main advantage of using a RRDE is the ability of simultaneously employing two separate conventional electrochemical techniques. This was achieved using bipotentiostatic mode for the measurements, where cyclic voltammetry was performed on the disk and chronoamperometry on the ring electrode, respectively. Thus, the glassy carbon disk modified with the GA/Fe^{III} capsules was subjected to a CV scan in the potential range starting from −450 to +700 mV, while the gold ring was kept at a constant potential of −450 mV that is sufficient for the reduction of Fe^{III} ions (**Figure S3**) that may be released into the solution.
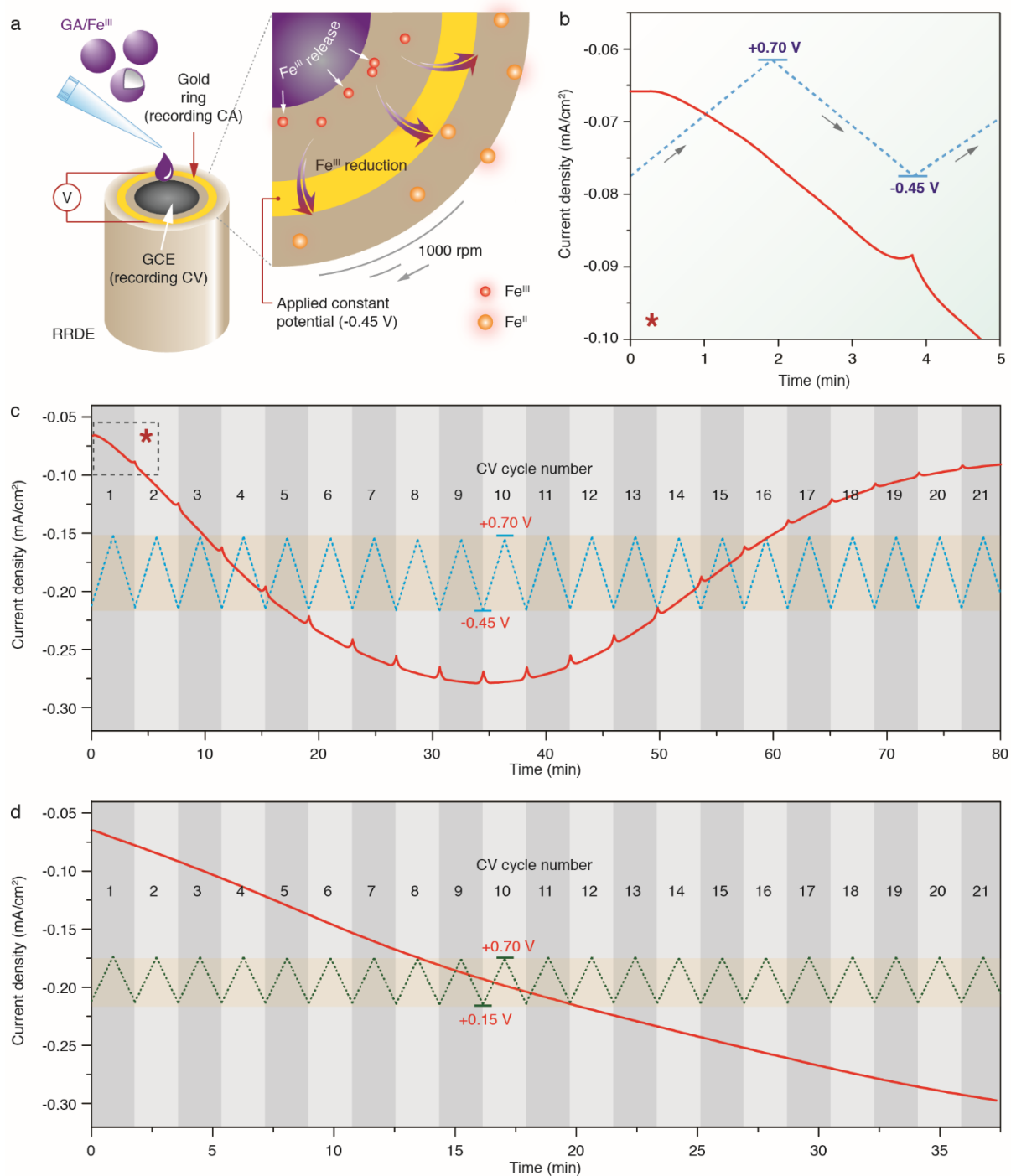
12

Figure 4. (a) Schematic representation of Fe^{III} release from the GA/Fe^{III} networks drop-cast on a glassy carbon disk and reduction of the released Fe^{III} to Fe^{II} at the gold ring of a RRDE. (b) Chronoamperogram recorded at the gold ring during the 1st CV cycle of the GA/Fe^{III} networks in the potential region ranging from −450 to +700 mV. Extended CA profiles of the GA/Fe^{III} networks measured during 21 consecutive CV cycles in the potential regions ranging (c) from

−450 to +700 mV and (d) from +150 to +700 mV. The speed of the RRDE was 1000 rpm, the scan rate was 10 mV/s, and the applied constant potential of the gold ring was −450 mV.

We hypothesize that upon oxidation of the GA/Fe^{III} networks, weakly coordinated Fe^{III} ions (owing to the Fe^{III}–quinone[40] complex formation upon oxidation of GA) are swept away from the networks drop-cast on the glassy carbon disk because of the physical disturbance caused by rotation of the electrode (1000 rpm) and driven to the gold ring electrode where they are reduced to Fe^{II}. According to the chronoamperometric (CA) profile recorded at the gold ring electrode (**Figure 4**b), the current increased with time (during the forward CV scan), which directly confirms the reduction of the Fe^{III} ions originating from the gradually oxidizing GA/Fe^{III} networks. The reduction current on the ring was measured nearly until the end of the reverse CV scan where the supply of Fe^{III} ions decreased. At this point, the Fe^{III} ions were simply reduced within the GA/Fe^{III} networks at the disc electrode, thereby lowering the amount of Fe^{III} ions available for further reduction at the ring electrode. This is reflected by the current drop in the recorded CA scan. At the beginning of the 2nd CV scan, the supply of Fe^{III} ions was restored (upon further oxidation of GA and the oxidation of newly formed Fe^{II}), and the process repeated itself (**Figure 4**c). The CA experiments were conducted at the ring electrode while simultaneously running 20 consecutive CV cycles (**Figure S4**) to obtain information regarding the stability of the GA/Fe^{III} networks under repetitive oxidation/reduction conditions. A repetitive local "on–off" characteristic Fe^{III} release was observed during the reductive and oxidative stimuli that induced the disassembly of the GA/Fe^{III} networks. The largest amount of Fe^{III} was released after ~35 min, with the GA/Fe^{III} networks being completely disassembled after 80 min under the electrochemical conditions studied herein. Furthermore, to assess whether continuous Fe^{III} ion release from the GA/Fe^{III} networks (hence, gradual disassembly of the networks) could be achieved, CV scans were run within a smaller potential window ranging from +150 to +700 mV to avoid reduction of the released Fe^{III} in the bulk solution to

Fe^{II}. GA in the GA/Fe^{III} networks is expected to be constantly oxidized in the forward cycle and to form a weaker Fe^{III}–quinone complex, from which Fe^{III} ions are released and can subsequently be monitored at the ring electrode. As in the previous case with a broad potential window, a constant potential of −450 mV was applied to the gold ring for recording the CA profile for 20 CV cycles (**Figure S5**) at the disk electrode (**Figure 4**d). As expected, we did not observe any disruption or "on–off"-type behavior in the Fe^{III} ion release on the recorded CA profile during repetitive cycling, as was the case with the broader potential range applied that would encompass the reduction of Fe^{III} ions from the bulk solution. Therefore, by avoiding Fe^{III} ion reduction in the networks while constantly oxidizing GA, continuous release of Fe^{III} ions from the GA/Fe^{III} networks can be achieved.

CONCLUSIONS

We have demonstrated that the MPN materials prepared from a simple phenolic ligand, GA, and Fe^{III} as a metal crosslinker, are electrochemically active, and their redox response is of a quasi-reversible character. Our results suggest that the initial redox responses of the GA/Fe^{III} networks originate from the irreversible oxidation of the ligands as well as the reversible reduction of the metal ions. Nevertheless, in the chosen potential regions studied, the MPN networks are not responsive to reductive stimuli unless oxidized beforehand. More specifically, the strong GA–Fe^{III} interactions can be weakened during ligand oxidation (~80% upon the 1st CV cycle), leading to the formation of less stable coordination complexes. Finally, we have showed qualitatively, that the release of Fe^{III} from the networks upon inducing electrochemical stimuli can be achieved. We have additionally demonstrated the specific redox conditions required for "on–off"- or continuous-type disassembly of the GA/Fe^{III} networks. Based on these results, various iron-dependent processes in the fields of agri/aquaculture and marine science may benefit from using a system, similar to ours, that is capable of supplying Fe^{III} on demand and in a controlled manner. Overall, our results unravel valuable fundamental insights

15

for the future design of multifunctional MPN platforms for various biologically relevant applications and may have implications for drug delivery whereby an oxidizing environment of sufficient redox potential will be required to weaken the coordinated phenolic networks. We are currently extending our investigation to other MPN systems, including the use of other simple phenolic ligands and different metal ions.

ASSOCIATED CONTENT

Supporting Information

The Supporting Information is available free of charge.

Differential interference contrast microscopy image of as-prepared GA/Fe^{III} capsules. Details on the changes in residual oxidation/reduction peak currents as a function of CV cycle number for the GA/Fe^{III} networks. Cyclic voltammogram of an FeCl$_3\cdot$6H$_2$O aqueous solution. Successive cyclic voltammograms of the GA/Fe^{III} networks recorded on a rotating ring-disk electrode.

AUTHOR INFORMATION

Corresponding Author

*E-mail: fcaruso@unimelb.edu.au.

Author Contributions

The manuscript was written through contributions of all authors. All authors have given approval to the final version of the manuscript.

Notes

The authors declare no competing financial interest.

ABBREVIATIONS

MPN, metal–phenolic networks; GA, gallic acid; PS, polystyrene; THF, tetrahydrofuran; CV, cyclic voltammogram; CA profile, chronoamperometric profile; GCE, glassy carbon electrode; RRDE, rotating ring-disk electrode.

REFERENCES

(1) Cui, Y.; Li, B.; He, H.; Zhou, W.; Chen, B.; Qian, G. Metal–Organic Frameworks as Platforms for Functional Materials. *Acc. Chem. Res.* **2016**, *49*, 483–493.

(2) Foo, M. L.; Matsuda, R.; Kitagawa, S. Functional Hybrid Porous Coordination Polymers. *Chem. Mater.* **2014**, *26*, 310–322.

(3) Kaushik, A.; Kumar, R.; Arya, S. K.; Nair, M.; Malhotra, B. D.; Bhansali, S. Organic–Inorganic Hybrid Nanocomposite-Based Gas Sensors for Environmental Monitoring. *Chem. Rev.* **2015**, *115*, 4571–4606.

(4) Zhang, J.; Su, C.-Y. Metal-Organic Gels: From Discrete Metallogelators to Coordination Polymers. *Coord. Chem. Rev.* **2013**, *257*, 1373–1408.

(5) Ejima, H.; Richardson, J. J.; Liang, K.; Best, J. P.; van Koeverden, M. P.; Such, G. K.; Cui, J.; Caruso, F. One-Step Assembly of Coordination Complexes for Versatile Film and Particle Engineering. *Science* **2013**, *341*, 154–157.

(6) Ejima, H.; Richardson, J. J.; Caruso, F. Phenolic Film Engineering for Template-Mediated Microcapsule Preparation. *Polym. J.* **2014**, *46*, 452–459.

(7) Guo, J.; Ping, Y.; Ejima, H.; Alt, K.; Meissner, M.; Richardson, J. J.; Yan, Y.; Peter, K.; von Elverfeldt, D.; Hagemeyer, C. E.; Caruso, F. Engineering Multifunctional Capsules through the Assembly of Metal–Phenolic Networks. *Angew. Chem., Int. Ed.* **2014**, *53*, 5546–5551.

(8) Rahim, M. A.; Björnmalm, M.; Suma, T.; Faria, M.; Ju, Y.; Kempe, K.; Müllner, M.; Ejima, H.; Stickland, A. D.; Caruso, F. Metal–Phenolic Supramolecular Gelation. *Angew. Chem., Int. Ed.* **2016**, *55*, 13803–13807.

(9) Rahim, M. A.; Kempe, K.; Müllner, M.; Ejima, H.; Ju, Y.; van Koeverden, M. P.; Suma, T.; Braunger, J. A.; Leeming, M. G.; Abrahams, B. F.; Caruso, F. Surface-Confined Amorphous Films from Metal-Coordinated Simple Phenolic Ligands. *Chem. Mater.* **2015**, *27*, 5825–5832.

(10) Rahim, M. A.; Björnmalm, M.; Bertleff-Zieschang, N.; Besford, Q.; Mettu, S.; Suma, T.; Faria, M.; Caruso, F. Rust-Mediated Continuous Assembly of Metal–Phenolic Networks. *Adv. Mater.* **2017**, *29*, 1606717.

(11) Bertleff-Zieschang, N.; Rahim, M. A.; Ju, Y.; Braunger, J. A.; Suma, T.; Dai, Y.; Pan, S.; Cavalieri, F.; Caruso, F. Biofunctional Metal–Phenolic Films from Dietary Flavonoids. *Chem. Commun.* **2017**, *53*, 1068–1071.

(12) Han, P.; Shi, J.; Nie, T.; Zhang, S.; Wang, X.; Yang, P.; Wu, H.; Jiang, Z. Conferring Natural-Derived Porous Microspheres with Surface Multifunctionality through Facile Coordination-Enabled Self-Assembly Process. *ACS Appl. Mater. Interfaces* **2016**, *8*, 8076–8085.

(13) Ju, Y.; Dai, Q.; Cui, J.; Dai, Y.; Suma, T.; Richardson, J. J.; Caruso, F. Improving Targeting of Metal–Phenolic Capsules by the Presence of Protein Coronas. *ACS Appl. Mater. Interfaces* **2016**, *8*, 22914–22922.

(14) Liang, H.; Li, J.; He, Y.; Xu, W.; Liu, S.; Li, Y.; Chen, Y.; Li, B. Engineering Multifunctional Films Based on Metal–Phenolic Networks for Rational pH-Responsive Delivery and Cell Imaging. *ACS Biomater. Sci. Eng.* **2016**, *2*, 317–325.

(15) Liang, H.; Zhou, B.; Li, J.; Xu, W.; Liu, S.; Li, Y.; Chen, Y.; Li, B. Supramolecular Design of Coordination Bonding Architecture on Zein Nanoparticles for pH-Responsive Anticancer Drug Delivery. *Colloids Surf., B* **2015**, *136*, 1224–1233.

(16) Meyer, C.; Ponzio, F.; Mathieu, E.; Ball, V. Kinetics of Deposition and Stability of Pyrocatechol –FeIII Coordinated Films. *Mater. Sci. Eng., C* **2017**, *72*, 620–624

(17) Abdel-Hamid, R.; Newair, E. F. Electrochemical Behavior of Antioxidants: I. Mechanistic Study on Electrochemical Oxidation of Gallic Acid in Aqueous Solutions at Glassy-Carbon Electrode. *J. Electroanal. Chem.* **2011**, *657*, 107–112.

(18) Hung, C. H.; Chang, W. T.; Su, W. Y.; Cheng, S. H. Electrochemical Determination of Pyrogallol at Conducting Poly(3,4-ethylenedioxythiophene) Film-Modified Screen-Printed Carbon Electrodes. *Electroanalysis* **2014**, *26*, 2237–2243.

(19) Nematollahi, D.; Rafiee, M. Electrochemical Oxidation of Catechols in the Presence of Acetylacetone. *J. Electroanal. Chem.* **2004**, *566*, 31–37.

(20) Anderson, A.; Davis, J. Electrochemical Actuators: Controlled Drug Release Strategies for Use in Micro Devices. *Electroanalysis* **2015**, *27*, 872–878.

(21) Lee, H.; Choi, T. K.; Lee, Y. B.; Cho, H. R.; Ghaffari, R.; Wang, L.; Choi, H. J.; Chung, T. D.; Lu, N.; Hyeon, T.; Choi, S. H.; Kim, D.-H. A Graphene-Based Electrochemical Device with Thermoresponsive Microneedles for Diabetes Monitoring and Therapy. *Nat. Nanotechnol.* **2016**, *11*, 566–572.

(22) Svirskis, D.; Travas-Sejdic, J.; Rodgers, A.; Garg, S. Electrochemically Controlled Drug Delivery Based on Intrinsically Conducting Polymers. *J. Controlled Release* **2010**, *146*, 6–15.

(23) Szunerits, S.; Teodorescu, F.; Boukherroub, R. Electrochemically Triggered Release of Drugs. *Eur. Polym. J.* **2016**, *83*, 467–477.

(24) Balhara, M.; Chaudhary, R.; Ruhil, S.; Singh, B.; Dahiya, N.; Parmar, V. S.; Jaiwal, P. K.; Chhillar, A. K. Siderophores; Iron Scavengers: The Novel and Promising Targets for Pathogen Specific Antifungal Therapy. *Expert Opin. Ther. Targets* **2016**, *20*, 1477–1489.

(25) Wilson, B. R.; Bogdan, A. R.; Miyazawa, M.; Hashimoto, K.; Tsuji, Y. Siderophores in Iron Metabolism: From Mechanism to Therapy Potential. *Trends Mol. Med.* **2016**, *22*, 1077–1090.

(26) Robinson, N. J.; Procter, C. M.; Connolly, E. L.; Guerinot, M. L. A Ferric-Chelate Reductase for Iron Uptake from Soils. *Nature* **1999**, *397*, 694–697.

(27) Guerinot, M. L.; Yi, Y. Iron: Nutritious, Noxious, and Not Readily Available. *Plant Physiol.* **1994**, *104*, 815–820.

(28) Grillet, L.; Mari, S.; Schmidt, W. Iron in Seeds – Loading Pathways and Subcellular Localization. *Front. Plant Sci.* **2014**, *4*, 1–8.

(29) Hutchins, D. A.; Witter, A. E.; Butler, A.; Luther, G. W. Competition among Marine Phytoplankton for Different Chelated Iron Species. *Nature* **1999**, *400*, 858–861.

(30) Cui, J.; Liu, Y.; Hao, J. Multiwalled Carbon-Nanotube-Embedded Microcapsules and Their Electrochemical Behavior. *J. Phys. Chem. C* **2009**, *113*, 3967–3972.

(31) Shchukin, D. G.; Köhler, K.; Möhwald, H. Microcontainers with Electrochemically Reversible Permeability. *J. Am. Chem. Soc.* **2006**, *128*, 4560–4561.

(32) Zheng, S.; Tao, C.; He, Q.; Zhu, H.; Li, J. Self-Assembly and Characterization of Polypyrrole and Polyallylamine Multilayer Films and Hollow Shells. *Chem. Mater.* **2004**, *16*, 3677–3681.

(33) Chen, P. C.; Chang, Y. M.; Wu, P. W.; Chiu, Y. F. Fabrication of Ni Nanowires for Hydrogen Evolution Reaction in a Neutral Electrolyte. *Int. J. Hydrogen Energy* **2009**, *34*, 6596–6602.

(34) Cherepanov, P. V.; Melnyk, I.; Skorb, E. V.; Fratzl, P.; Zolotoyabko, E.; Dubrovinskaia, N.; Dubrovinsky, L.; Avadhut, Y. S.; Senker, J.; Leppert, L.; Kummel, S.; Andreeva, D. V. The Use of Ultrasonic Cavitation for Near-Surface Structuring of Robust and Low-Cost AlNi Catalysts for Hydrogen Production. *Green Chem.* **2015**, *17*, 2745–2749.

(35) Cherepanov, P. V.; Andreeva, D. V. In *Handbook of Ultrasonics and Sonochemistry*; Ashokkumar, M., Ed.; Springer Singapore: Singapore, 2016; Chapter 17, pp 525–552.

(36) Brett, A. M. O.; Ghica, M. E. Electrochemical Oxidation of Quercetin. *Electroanalysis* **2003**, *15*, 1745–1750.

(37) Nkhili, E.; Loonis, M.; Mihai, S.; El Hajji, H.; Dangles, O. Reactivity of Food Phenols with Iron and Copper Ions: Binding, Dioxygen Activation and Oxidation Mechanisms. *Food Funct.* **2014**, *5*, 1186–1202.

(38) Borgias, B. A.; Cooper, S. R.; Koh, Y. B.; Raymond, K. N. Synthetic, Structural, and Physical Studies of Titanium Complexes of Catechol and 3,5-Di-*tert*-Butylcatechol. *Inorg. Chem.* **1984**, *23*, 1009–1016.

(39) Cooper, S. R.; McArdle, J. V.; Raymond, K. N. Siderophore Electrochemistry: Relation to Intracellular Iron Release Mechanism. *Proc. Natl. Acad. Sci. U. S. A.* **1978**, *75*, 3551–3554.

(40) Hider, R. C.; Liu, Z. D.; Khodr, H. H. Metal Chelation of Polyphenols. *Methods Enzymol.* **2001**, *335*, 190–203.
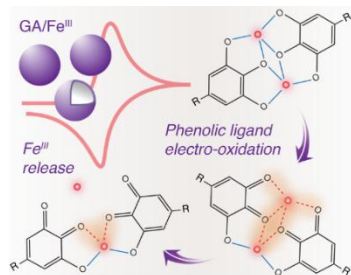
TOC Image

Author/s:
Cherepanov, PV; Rahim, MA; Bertleff-Zieschang, N; Abu Sayeed, M; O'Mullane, AP; Moulton, SE; Caruso, F

Title:
Electrochemical Behavior and Redox-Dependent Disassembly of Gallic Acid/Fe-III Metal-Phenolic Networks

Date:
2018-02-14

Persistent Link:
http://hdl.handle.net/11343/198313

File Description:
Accepted version